Published in final edited form as:
Magn Reson Med. 2009 December ; 62(6): 1457–1465. doi:10.1002/mrm.22091.

High-Frequency Mode Conversion Technique for Stiff Lesion Detection with Magnetic Resonance Elastography

Yogesh K Mariappan[1,†], **Kevin J Glaser**[1], **Armando Manduca**[2], **Anthony J Romano**[3], **Sudhakar K Venkatesh**[4], **Meng Yin**[1], and **Richard L Ehman**[1,*]

[1]Department of Radiology, Mayo Clinic, Rochester, MN, USA

[2]Biomathematics Resource, Mayo Clinic, Rochester, MN, USA

[3]Naval Research Laboratory, Washington, DC, USA

[4]Department of Diagnostic Radiology, Yong Loo Lin School of Medicine, National University of Singapore, Singapore

Abstract

A novel imaging technique is described in which the mode conversion of longitudinal waves is used for the qualitative detection of stiff lesions within soft tissue using Magnetic Resonance Elastography (MRE) methods. Due to the viscoelastic nature of tissue, high-frequency shear waves attenuate rapidly in soft tissues but much less in stiff tissues. By introducing minimally attenuating longitudinal waves at a significantly high frequency into tissue, shear waves produced at interfaces by mode conversion will be detectable in stiff regions, but will be significantly attenuated and thus not detectable in the surrounding soft tissue. This contrast can be used to detect the presence of stiff tissue. The proposed technique is shown to readily depict hard regions (mimicking tumors) present in tissue-simulating phantoms and ex vivo breast tissue. In vivo feasibility is demonstrated on a patient with liver metastases where the tumors are readily distinguished. Preliminary evidence also suggests that quantitative stiffness measurements of stiff regions obtained with this technique are more accurate than those from conventional MRE because of the short shear wavelengths. This rapid, qualitative technique may lend itself to applications in which the localization of stiff, suspicious neoplasms is coupled with more sensitive techniques for thorough characterization.

Keywords

MR Elastography; high-frequency MRE; mode conversion; stiff lesion detection; stiffness

Introduction

Dynamic Magnetic Resonance Elastography (MRE, (1,2)) is a phase-contrast MRI-based technique for quantitatively mapping the shear modulus of tissues. This technique is now being used clinically for the assessment of liver fibrosis (3,4) and is being investigated for imaging other organs, such as the breast, brain, and prostate (5-7). In MRE, vibrations are often applied to the tissue of interest using an external mechanical wave driver, and the

[†]**Correspondence for review comments and proofs:** Yogesh K. Mariappan, Department of Radiology, Mayo Clinic, 200 First Street SW, Rochester, MN 55905, Phone: (507)-284-1112, Fax: (507)-284-9778, Mariappan.Yogesh@mayo.edu . [*]**Correspondence for published manuscript:** Richard L. Ehman, M.D., Department of Radiology, Mayo Clinic, 200 First Street SW, Rochester, MN 55905, Phone: (507)-284-9770, Fax: (507)-284-9778, Ehman.Richard@mayo.edu .

resulting motion is encoded in the phase of the transverse magnetization with the help of synchronized motion-sensitizing gradients inserted into conventional MR imaging pulse sequences. This process yields images of the propagating shear waves, which are processed with inversion algorithms to create images depicting mechanical properties of the tissue such as stiffness and viscosity (8,9).

Typically in these experiments, shear waves with frequencies in the range of 50-200 Hz are induced in the tissue either directly by using shear drivers (drivers that oscillate transversely to the tissue surface) or indirectly by using longitudinal drivers oscillating perpendicular to the tissue surface which produce shear waves within the tissue by mode conversion. Mechanical waves of higher frequencies are not generally used in MRE experiments since, as the frequency of vibration increases, the attenuation of the waves increases and the depth of penetration of the waves decreases. As described in the following section, this results in complete attenuation of shear waves above a cutoff frequency that is dependent upon the tissue properties and the cutoff frequency typically rises with tissue stiffness.

Since malignant tumors are often much stiffer than surrounding normal tissues, we have sought to exploit the high-frequency shear wave cutoff phenomenon as a way to preferentially visualize shear waves in tumors. We hypothesized that if longitudinal vibrations that are above the shear wave cutoff frequency of normal soft tissues are applied, then shear waves might be observed only in stiffer tissues, such as tumors. While adequate shear wave illumination is important for quantitative assessment of the tissue properties for an entire organ, this technique might be useful for the qualitative detection of tumors and other stiff lesions. The purpose of this work was to test this hypothesis in tissue-simulating phantoms and in ex vivo and in vivo tissue experiments, and to investigate the advantages and challenges of this technique.

Theory

The basic contrast mechanism of the proposed technique is the differential attenuation of shear waves in stiff and soft materials. If planar shear waves are introduced into a sample, the wavelength λ of the shear waves depends upon the shear wave speed v_s in the material and the frequency f of the shear waves according to $\lambda = v_s / f$. The wave speed and the attenuation α (per unit distance in the direction of propagation) of the waves are related to the complex shear modulus μ of the medium (10), and can be written as

$$v_s^2 = \frac{2\left(\mu_r^2+\mu_i^2\right)}{\rho\left(\mu_r+\sqrt{\mu_r^2+\mu_i^2}\right)}; \alpha^2 = \frac{\rho\omega^2\sqrt{\mu_r^2+\mu_r^2}-\mu_r}{2\left(\mu_r^2+\mu_r^2\right)}$$

where μ_r and μ_i are the real and imaginary parts of the shear modulus, $\omega = 2\pi f$, and ρ is the density (assumed to be 1000 kg/m^3). The above equations are model independent, but to simplify the analysis, a simple Voigt model with $\mu = c + i\omega\eta$, where c is the static shear modulus and η is the frequency-independent shear viscosity, was used in this work. The shear stiffness typically reported in MRE is related to ρv_s^2, which provides a convenient estimate of the effective shear modulus at a particular frequency. If the frequency of the shear waves is increased, the wavelength decreases while the wave attenuation increases. For instance, the single MRE wave image in Fig. 1a shows a uniform gel phantom illuminated with shear waves at 150 Hz. Compared to the wave images shown in Figs. 1b and 1c indicating the shear wave propagation in the same phantom at 300 and 450 Hz, respectively, it can be seen that the wavelength and the depth of the wave penetration decrease as the frequency increases. If the shear wave frequency is further increased, above a certain frequency the attenuation of the waves would be so high that shear waves would not be detectable in the phantom. Since the attenuation of the waves for a given distance of propagation is generally less in stiff media than it is in softer media

(11), this upper "cutoff" frequency at which the shear waves disappear depends upon the stiffness of the medium and is higher for stiff media.

In the conventional low-frequency range for MRE, both stiff and soft tissues have significant wave amplitude, whereas if very high frequency waves are used, the attenuation is too high to image the waves anywhere in the tissue. Therefore, it is desirable to use a frequency just high enough to extinguish the waves in the soft tissues while still being able to image the waves in the stiffer regions. To predict the frequency that needs to be used to distinguish stiff regions from soft background tissue, a theoretical model was used in which a planar shear wave attenuates exponentially as it propagates in a medium (i.e., the wave attenuates according to $e^{-\alpha r}$, were α is the attenuation factor and r is the distance in the direction of propagation). Since the wave is assumed to decay exponentially, mathematically the amplitude will reach zero only at infinity. For practical purposes, it is assumed that if the wave amplitude reaches $1/100^{th}$ of its original amplitude (i.e., the wave undergoes 99% decay) in a distance of 5 mm, then the wave is effectively attenuated and the frequency at which this occurs is referred to as the "critical frequency" f_c for that particular material ($\alpha(f_c) = -\ln(1/100)/(0.005\text{ m}) \approx 921\text{ m}^{-1}$). By introducing longitudinal vibrations into tissue at a frequency above the critical frequency for the softer surrounding tissue, shear waves produced in the soft tissue due to mode conversion at the boundaries and internal surfaces will not be readily detectable, whereas the shear waves produced in stiff regions in the tissue will be visible and will indicate the presence of the stiff regions.

Methods

A series of phantom studies were designed to test the hypothesis that it is possible to detect stiff regions inside a softer medium with the help of high-frequency mode-converted shear waves and to test the validity of the theoretical model. A 1.5-Tesla whole-body scanner (GE Healthcare, Milwaukee, WI) was used for all the experiments. To induce the mechanical vibrations in the gelatin phantoms, an electromechanical driver capable of longitudinal vibrations was used (Fig. 2a). When an alternating electric current is sent through the voice coil of the driver, a local magnetic moment created perpendicular to the main magnetic field tries to align with the main field B_0, moving the flexible platform vertically. When the current reverses, the platform deflects in the other direction. This motion of the platform is coupled to the sample with the help of the drive shaft and the contact plate attached to it. Figure 2a also shows a schematic of a typical two-part phantom made up of 10% bovine gel (Sigma Life Sciences, MO, USA) to simulate normal soft tissue and a 4% agar gel (DIFCO, MI, USA) inclusion, located away from the contact plate, simulating a stiff lesion. A spin-echo MRE pulse sequence was used to acquire wave data within a coronal imaging plane using motion-encoding gradient pairs with an amplitude of 4 G/cm to sensitize to the wave motion in the direction perpendicular to the imaging plane. Various mechanical excitation frequencies from 60-1500 Hz were used to study the wave propagation in both media, and the number of motion-encoding gradient pairs was adjusted to have approximately one gradient pair per 100-Hz frequency in each case (motion-encoding time of 10-17 ms). Other typical MRE imaging parameters for the phantom experiments were 24-cm FOV, 256×128 acquisition matrix, 300-ms TR, 46-ms TE, 16-kHz receiver bandwidth, 1 NEX, 10-mm slice thickness, 4 time offsets and 5 minutes total scan time. Since the wave fields created are a combination of the induced longitudinal waves and the mode-converted shear waves of interest, Gaussian band-pass filters with bounds of 5 and 100 cycles per field of view were used to remove the low-spatial-frequency longitudinal waves and the high-frequency noise.

To demonstrate that the shear waves created in the stiff inclusion by mode conversion at the boundaries between the stiff and soft media are similar to shear waves directly induced within the stiff inclusion, the drive shaft and contact plate were replaced by a silver needle

attached to the flexible platform (similar to (12)) and inserted into the stiff inclusion through the soft surrounding gel. When the alternating current flows through the voice coil, the needle moves up and down in the inclusion directly inducing shear waves inside it. This minimally invasive needle driver technique was the simplest way to directly induce shear waves inside the stiff region. Shear waves with the same range of frequencies as above were induced in the inclusion, imaged with the aforementioned pulse sequence, and compared to the shear waves created by the mode conversion of longitudinal waves using the original experimental setup.

Images of stiffness estimates (elastograms) were calculated using the local frequency estimation (LFE) algorithm (8) with the application of spatio-temporal directional filtering (13) for both the standard low-frequency MRE and the high-frequency MRE data. To test the validity of the theoretical model, data were collected in the inclusion phantom using the longitudinal driver at several frequencies from 100-1000 Hz. From the wave data obtained, wave amplitude maps were derived and wave attenuation factors were calculated in regions where planar shear waves could be approximated and these attenuation values were compared to the theoretically predicted values.

To assess the feasibility of this technique in real tissues, experiments were performed on an ex vivo, formalin-fixed breast specimen. To simulate a stiff lesion in this specimen, a small volume within the specimen was ablated with focused ultrasound (FUS). The experimental setup and imaging parameters were similar to the phantom experiments. The contact plate was placed directly on top of the specimen and used to induce longitudinal waves at 50-1500 Hz within the tissue.

To demonstrate the feasibility of this technique for in vivo imaging, the technique was tested on a healthy volunteer and a patient with a malignant liver tumor in accordance with the Mayo Clinic Institutional Review Board. The patient had metastatic tumors in an otherwise normal liver (i.e., not cirrhotic and with no detectable fibrosis) and underwent clinical MRE performed at 60 Hz to assess liver and tumor tissue stiffness. Due to the limitations of the mechanical driver used for clinical MRE in the high-frequency range, a frequency of 200 Hz was used for the high-frequency experiments. The clinically used mechanical wave driver, shown schematically in Fig. 2b, is a pressure-activated driver in which mechanical waves of the required frequency created by an active audio speaker are coupled to the abdomen through a passive driver placed on the chest wall. This produces longitudinal motion which is converted into shear waves by mode conversion from various tissue interfaces within the abdomen (14). To compare the results obtained from the patient experiment to a control case, a healthy volunteer also underwent MRE at 60 Hz and 200 Hz. A gradient-echo MRE pulse sequence and a 8-channel torso array coil were used for wave data acquisition. Other MRE imaging parameters included an axial slice orientation, 36-cm FOV, 256×64 acquisition matrix, 50-ms TR, echo times of 24.2 and 27.5 ms for the 60-Hz and 200-Hz acquisitions respectively, 30° flip angle, 16-kHz receiver bandwidth, 1 NEX, 5-mm slice thickness, 4 time offsets and 19.6 s total scan time.

Results

From the data obtained at multiple frequencies, the Voigt model parameters were calculated by a least squares fit of wave speed (v_s) as a function of the operating frequencies (15) and these were found to be (c,η) = (3.0 kPa, 1.36 Pa-s) for the B-gel and (120 kPa, 10.2 Pa-s) for the agar. Figure 3a shows plots of the attenuation factor for B-gel and agar as a function of excitation frequency. The stiffer gel can be seen to have less attenuation than the softer gel. Figure 3b shows plots of the decay distance for each gel at the same frequencies. Because of

its increased attenuation, the waves in the softer gel decay more rapidly than in the stiffer gel. From the figure, the B-gel can be seen to have a critical frequency of about 723 Hz.

A magnitude image of the cross section of the inclusion phantom through the inclusion is shown in Fig. 4a, where the presence of the inclusion can be identified as the hypointense region near the middle of the phantom. The mechanical vibrations were applied in a direction perpendicular to the plane of this image and Fig. 4b shows a single band-pass filtered wave image of the phantom with 60-Hz longitudinal waves produced in it. The waves visible in Fig. 4b are the mode-converted shear waves produced at the phantom and inclusion boundaries. The stiff region cannot be distinguished from the soft background region simply by observation in these wave images (without the application of inversion algorithms). Figure 4c shows a single wave image of the same phantom with 750-Hz mechanical waves. From these data, the presence of the stiff region can be easily identified since only the stiff region shows the presence of the shear waves created at the interface between the background and the inclusion region. Some residual low spatial frequency waves and edge artifacts due to the band-pass filtering are also visible in the background gel in this image.

Data comparing the shear waves created in the stiff inclusion by mode conversion at the interfaces and by direct induction via the needle driver are shown in Fig. 5. Figures 5a and 5b show wave data obtained from the high-frequency needle driver experiment and the high-frequency mode-conversion experiment, respectively. Both datasets were obtained at 1000 Hz and the wavelengths of the shear waves present inside the inclusion in both cases are similar. With the needle driver, due to the imperfect insertion and wobbling of the tip of the needle, the wave pattern was not perfectly symmetric. Furthermore, by inspecting the multiple wave images obtained at equally spaced time points over a single wave period (not shown), it could be noted that in the needle-driver case, the shear waves originated from the needle insertion point and moved away towards the border of the inclusion. When they reached the interface, due to the high stiffness mismatch, almost no waves were transmitted into the soft region. However, with the high-frequency longitudinal driver data, shear waves were created at the interface between the soft and stiff regions and traveled away from the interface in both directions (i.e., both towards the center of the inclusion and towards the boundary of the phantom). This bidirectional propagation pattern is evident in the zoomed single wave image shown in Fig. 5c. The shear waves that travel toward the center of the inclusion increase in wave amplitude due to constructive interference while the waves that are moving away from the interface within the soft region have very short wavelengths and their amplitudes reduce quickly, in accordance with the theoretical prediction that shear waves of frequencies higher than the critical frequency (723 Hz) would extinguish very quickly inside the soft region.

Figures 6a and 6b show stiffness images (elastograms) obtained from the conventional low-frequency and the high-frequency MRE experiments, respectively, whose corresponding wave data are shown in Figs. 4b and 4c, respectively. Based on the Voigt model parameters, the stiffness of the 4% agar gel was estimated to be 120.1 and 134 kPa for the 60 and 750 Hz experiments. However, the shear stiffness as obtained from the low-frequency 60-Hz MRE experiment was 6.2 kPa. This underestimation can be attributed to the wavelength of the shear waves being much larger than the dimensions of the inclusions (8). The stiffness value obtained from the 750-Hz experiment in the inclusion was 142 kPa, demonstrating that high-frequency MRE can more accurately assess the mechanical properties of stiff regions than conventional low-frequency MRE.

The two curves with and without markers shown in Fig. 7a indicate the change of the attenuation factor with respect to increasing frequencies for the experimental wave data and

the theoretical model of the soft background gel, respectively. The attenuation factor for the experimental data is shown only for the frequency range of 100-750 Hz since reliable estimation of the attenuation factor could not be performed above 750 Hz due to the heavy attenuation of the waves at these higher frequencies. Figure 7b shows a different representation of the same data, where the distances required for 99% decay of the wave amplitude based on the attenuation factors in Fig. 7a for the theoretical model and the experimental data are shown. The experimental observations follow the theoretical predictions closely.

Data obtained from the ex vivo specimen experiment are shown in Fig. 8. A conventional MR magnitude image is shown in Fig. 8a, where the position of the focused-ultrasound-ablated stiff region is indicated with the dotted line at the boundary. Voigt-model fit coefficients for this formalin-fixed breast specimen were found to be c,η = 16.3 kPa, 9.36 Pa-s. The vibrational energy was applied in the direction perpendicular to the imaging plane. A single wave image of the phantom at a conventional low frequency of 200 Hz is shown in Fig. 8b. The stiff region could not be detected simply by inspection of the wave images. For the Voigt-model values, the critical frequency was predicted to be 2815 Hz, but due to the limitation of the driver at this frequency, a frequency of 1000 Hz was used for the high-frequency experiments. The stiff FUS-ablated region can be easily differentiated from the soft breast tissue, as is evident from the wave image shown in Fig. 8c, due to the presence of shear waves exclusively in the lesion. Since a frequency lower than the critical frequency was used, low-wavelength shear waves are also visible in the softer outer region more than 5 mm away from the boundary.

Data from the preliminary in vivo study performed on a patient with stiff metastatic tumors (16) in an otherwise normal liver is shown in Fig. 9 compared to data obtained from a volunteer with a normal healthy liver. Figures 9a and 9d show the axial magnitude images of both the volunteer and the patient, respectively. In this particular case, the tumor within the liver of the patient could be distinguished in the magnitude image itself (arrow). Figures 9b and 9e show wave images at the conventional liver MRE frequency (60 Hz) in the healthy liver and the diseased liver, respectively. Variations in the wavelength and wave propagation in the diseased liver are observable in this case indicating substantial heterogeneity of the liver. Voigt-model fit coefficients for normal hepatic tissue have been determined to be c,η = 2 kPa, 1.9 Pa-s (17), which correspond to a critical frequency of 690 Hz. However, as mentioned before, these high-frequency experiments were performed at 200 Hz due to driver limitations. The wave data using this relatively high frequency of 200 Hz indicate that in the normal liver (Fig. 9c) there are almost no shear waves present due to the highly attenuating nature of healthy liver tissue. However, in the patient data (Fig. 9f), shear waves are present in the tumor region while they have attenuated heavily (though not completely) in other regions, indicating that the tumor is stiff in comparison to other parts of the liver. The region of the tumor is better highlighted in the 200-Hz wave images than it is in the 60-Hz wave images.

Discussion

The results demonstrate that it is possible to implement a simple technique that can depict stiff regions present inside a softer medium based on the difference in shear wave attenuation characteristics of the two materials. This could potentially be a simple and fast technique for stiff lesion detection and hence might be used as a localizer to quickly locate suspicious regions that could be further interrogated as needed to characterize the tissue. Since the shear waves that are imaged with this technique are created by the mode conversion of longitudinal waves, which can propagate further and more easily in tissue than shear waves, organs that are located farther from the surface of the body and are otherwise

not accessible with directly induced shear waves could be analyzed with this technique. Furthermore, due to the smaller wavelengths of the shear waves used in this technique, the accuracy of the shear stiffness estimates of small stiff lesions obtained from these data could be better than those from conventional low-frequency MRE. Though the accuracy of the Voigt model for the behavior of biological tissues is still in contention (18-20) and the attenuation model used to define the critical frequency is just one of many possible choices, the essential principle of differential wave attenuation is valid irrespective of the rheological and wave propagation models that are chosen, which would only alter the specific value of the critical frequency. The phantom results shown in Fig. 7 which demonstrate good agreement between the theoretical wave attenuation model and the measured attenuation support the material and wave propagation models assumed in this work and justified their use for the tissue studies.

As a qualitative imaging technique, it would only be necessary to obtain a wave image at a single time point with this technique to provide enough evidence for the presence of a stiff region in tissue, unlike conventional MRE where multiple wave images are usually necessary. This would substantially reduce the acquisition time for this method compared to conventional low-frequency MRE. Depending on the operating frequency for this method for a particular application, the amplitude of the driver system at that frequency, and the hardware capabilities of the MR scanner, the use of high-frequency (i.e., short-duration) motion-encoding gradients in this method could result in reduced echo times compared to low-frequency MRE. This could potentially improve the image SNR and make the technique well suited for low-T2 tissues.

There are also some potential disadvantages associated with this high-frequency technique. For example, even though the accuracy of the stiffness measurements of stiff regions can improve using this technique, since there are no shear waves present in the soft regions, the quantitative stiffness information of the surrounding medium is lost, as is evident from Fig. 6b. Furthermore, the shear wave amplitude in the stiff regions can be low because the waves are at higher frequencies that are less efficiently produced and transmitted through soft tissue and are created by mode conversion that only converts a fraction of the incident longitudinal wave energy into shear waves. The mode conversion efficiency is dependent upon different parameters such as the angle of incidence and proximity to the source. However, the specifics were not addressed in this study and are the subjects of further research. However, these limitations could be partially rectified, for example, by increasing the amplitude of the applied longitudinal waves (within safety limits, (21)), or by applying an array of drivers to create a higher amplitude wave field due to constructive interference (22). Even after increasing the amplitude at these higher frequencies, patient comfort during this exam could be as good or better than for conventional low-frequency MRE.

Further work is needed to explore clinical applications of this technique. We expect the technique to potentially be complementary to contrast-enhanced MRI (23) in breast imaging. It may eventually be possible to develop this technique to serve clinical needs ranging from the detection of lung tumors to locating blood vessel calcifications. However, for the clinical application of this technique, mechanical drivers that can produce high-amplitude longitudinal waves at these high frequencies must be developed. Investigations are currently underway to achieve this goal.

Conclusions

From the results shown in this study, it is concluded that stiff regions in softer background media can be detected by exciting the media with high-frequency longitudinal waves and imaging the mode-converted shear waves that are exclusively present in the stiff regions.

Since the shear waves are created due to mode conversion of longitudinal waves, it could be possible to study stiff tissues and regions of tissues deep within the body than are difficult to analyze with conventional low-frequency MRE. The shear waves in the targeted stiff regions at high frequencies have much shorter wavelengths than at conventional frequencies, from which more accurate stiffness measurements can be obtained.

Acknowledgments

The authors thank Ingrid Menegezzo for help in performing some of the phantom studies.

References

1. Muthupillai R, Lomas DJ, Rossman PJ, Greenleaf JF, Manduca A, Ehman RL. Magnetic resonance elastography by direct visualization of propagating acoustic strain waves. Science 1995;269(5232): 1854–1857. [PubMed: 7569924]
2. Muthupillai R, Rossman PJ, Lomas DJ, Greenleaf JF, Riederer SJ, Ehman RL. Magnetic resonance imaging of transverse acoustic strain waves. Magn Reson Med 1996;36(2):266–274. [PubMed: 8843381]
3. Venkatesh, S.; Yin, M.; Talwalkar, J.; Ehman, R. Application of Liver MR Elastography in Clinical Practice; Proceedings 16th Scientific Meeting, International Society for Magnetic Resonance in Medicine; 2008 April; p. 2611
4. Yin M, Talwalkar JA, Glaser KJ, Manduca A, Grimm RC, Rossman PJ, Fidler JL, Ehman RL. Assessment of Hepatic Fibrosis With Magnetic Resonance Elastography. Clinical Gastroenterology and Hepatology 2007;5(10):1207–1213.e1202.. [PubMed: 17916548]
5. Sinkus R, Tanter M, Xydeas T, Catheline S, Bercoff J, Fink M. Viscoelastic shear properties of in vivo breast lesions measured by MR elastography. Magnetic Resonance Imaging 2005;23:159–165. [PubMed: 15833607]
6. Sack I, Beierbach B, Hamhaber U, Klatt D, Braun J. Non-invasive measurement of brain viscoelasticity using magnetic resonance elastography. NMR Biomed 2008;21(3):265–271. [PubMed: 17614101]
7. Kemper J, Sinkus R, Lorenzen J, Nolte-Ernsting C, Stork A, Adam G. MR elastography of the prostate: initial in vivo application. RoFo; Fortschritte auf dem Gebiete der Rontgenstrahlen und der Nuklearmedizin 2004;176(8):1094–1099.
8. Manduca A, Oliphant TE, Dresner MA, Mahowald JL, Kruse SA, Amromin E, Felmlee JP, Greenleaf JF, Ehman RL. Magnetic resonance elastography: non-invasive mapping of tissue elasticity. Med Image Anal 2001;5(4):237–254. [PubMed: 11731304]
9. Van Houten EE, Miga MI, Weaver JB, Kennedy FE, Paulsen KD. Three-dimensional subzone-based reconstruction algorithm for MR elastography. Magnetic Resonance in Medicine 2001;45(5): 827–837. [PubMed: 11323809]
10. Auld BA. Acoustic Fields and Waves in Solids. 1990
11. Yin, M.; Venkatesh, S.; Mariappan, Y.; Glaser, K.; Grimm, R.; Manduca, A.; Romano, A.; Ehman, R. Value of Shear Wave Attenuation as a Tissue Characterization Parameter in MR Elastography of the Liver; Proceedings 16th Scientific Meeting, International Society for Magnetic Resonance in Medicine; Toronto. 2008 April; p. 84
12. Chan QC, Li G, Ehman RL, Grimm RC, Li R, Yang ES. Needle shear wave driver for magnetic resonance elastography. Magn Reson Med 2006;55(5):1175–1179. [PubMed: 16528708]
13. Manduca A, Lake DS, Kruse SA, Ehman RL. Spatio-temporal directional filtering for improved inversion of MR elastography images. Medical Image Analysis 2003;7(4):465–473. [PubMed: 14561551]
14. Yin M, Rouviere O, Ehman RL. Diffraction-biased shear wave fields generated with longitudinal magnetic resonance elastography drivers. Magn Reson Imaging 2005;26(6):770–780. [PubMed: 18467059]

15. Kruse SA, Smith JA, Lawrence AJ, Dresner MA, Manduca A, Greenleaf JF, Ehman RL. Tissue characterization using magnetic resonance elastography: preliminary results. Physics in Medicine and Biology 2000;45:1579–1590. [PubMed: 10870712]

16. Venkatesh SK, Yin M, Glockner JF, Takahashi N, Araoz PA, Talwalkar JA, Ehman RL. MR elastography of liver tumors: preliminary results. AJR Am J Roentgenol 2008;190(6):1534–1540. [PubMed: 18492904]

17. Huwart L, Sempoux C, Salameh N, Jamart J, Annet L, Sinkus R, Peeters F, ter Beek LC, Horsmans Y, Van Beers BE. Liver Fibrosis: Noninvasive Assessment with MR Elastography versus Aspartate Aminotransferase to-Platelet Ratio Index. Radiology 2007;245(2):458–466. [PubMed: 17940304]

18. Catheline S, Gennisson JL, Delon G, Fink M, Sinkus R, Abouelkaram S, Culioli J. Measuring of viscoelastic properties of homogeneous soft solid using transient elastography: an inverse problem approach. J Acoust Soc Am 2004;116(6):3734–3741. [PubMed: 15658723]

19. Asbach P, Klatt D, Hamhaber U, Braun J, Somasundaram R, Hamm B, Sack I. Assessment of liver viscoelasticity using multifrequency MR elastography. Magn Reson Med 2008;60(2):373–379. [PubMed: 18666132]

20. Sinkus R, Siegmann K, Xydeas T, Tanter M, Claussen C, Fink M. MR elastography of breast lesions: understanding the solid/liquid duality can improve the specificity of contrast-enhanced MR mammography. Magn Reson Med 2007;58(6):1135–1144. [PubMed: 17969009]

21. Ehman EC, Rossman PJ, Kruse SA, Sahakian AV, Glaser KJ. Vibration safety limits for magnetic resonance elastography. Phys Med Biol 2008;53(4):925–935. [PubMed: 18263949]

22. Mariappan YK, Rossman PJ, Glaser KJ, Manduca A, Ehman RL. Magnetic resonance elastography with a phased-array acoustic driver system. Magn Reson Med 2009;61(3):678–685. [PubMed: 19132758]

23. Heywang-Kobrunner SH, Viehweg P, Heinig A, Kuchler C. Contrast-enhanced MRI of the breast: accuracy, value, controversies, solutions. European Journal of Radiology 1997;24(2):94–108. [PubMed: 9097051]

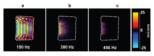

Figure 1.
Wave images of a homogeneous 16% bovine gel phantom with shear waves at (a) 150 Hz, (b) 300 Hz, and (c) 450 Hz. The boundary of the phantom is shown with the dotted line. The wavelength and penetration depth of the shear waves decrease while the attenuation increases with increasing frequency.

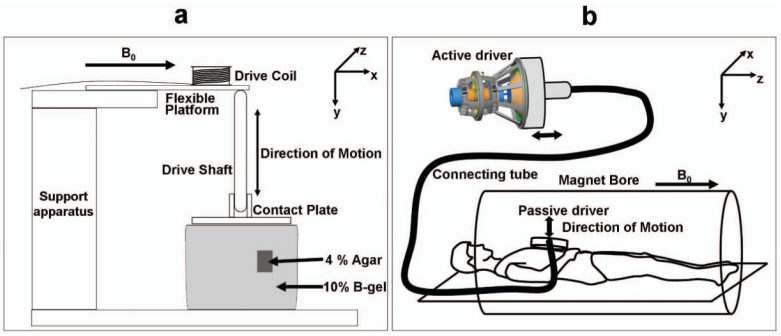

Figure 2.

(a) Schematic of the electromechanical driver and inclusion phantom used for the phantom experiments. (b) Schematic of the pressure activated driver system used for the in vivo human studies.

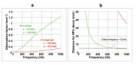

Figure 3.
(a) Changes in the attenuation factor with increasing excitation frequencies for 10% B-gel (green) and 4% agar (red). (b) The distance required for 99% decay of the shear wave amplitude for the B-gel (green) and agar (red) as a function of increasing frequency.

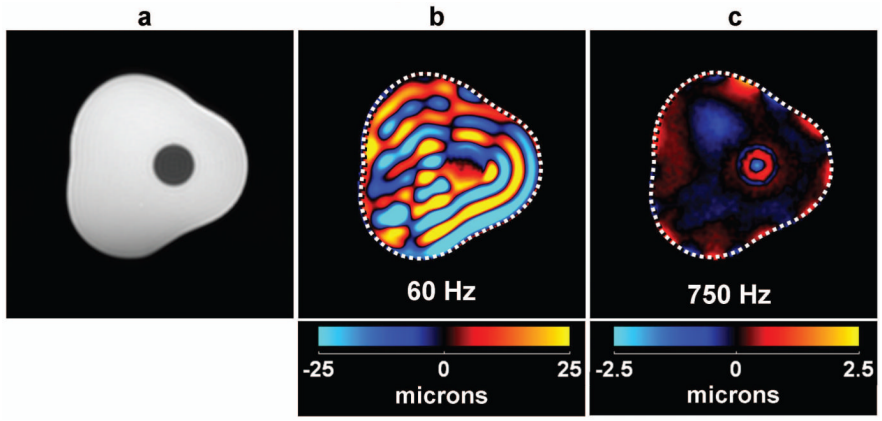

Figure 4.

(a) A conventional MR magnitude image of a cross section of the inclusion phantom showing the location of the inclusion as the hypointense region near the middle of the image. (b) A single wave image of the shear waves produced from 60-Hz longitudinal vibrations in the direction perpendicular to the imaging plane. (c) A single wave image due to 750-Hz longitudinal vibrations with the inclusion now clearly distinguishable from the background gel.

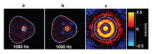

Figure 5.
(a) A single wave image of an inclusion phantom showing shear waves produced directly in the inclusion at 1000 Hz. (b) A wave image showing mode-converted shear waves in the inclusion due to 1000-Hz longitudinal vibrations applied at the surface of the phantom. (c) A magnified version of (b) highlighting the short- and long-wavelength shear waves in the soft and stiff regions, respectively. The boundary of the inclusion is indicated by the dotted circle.

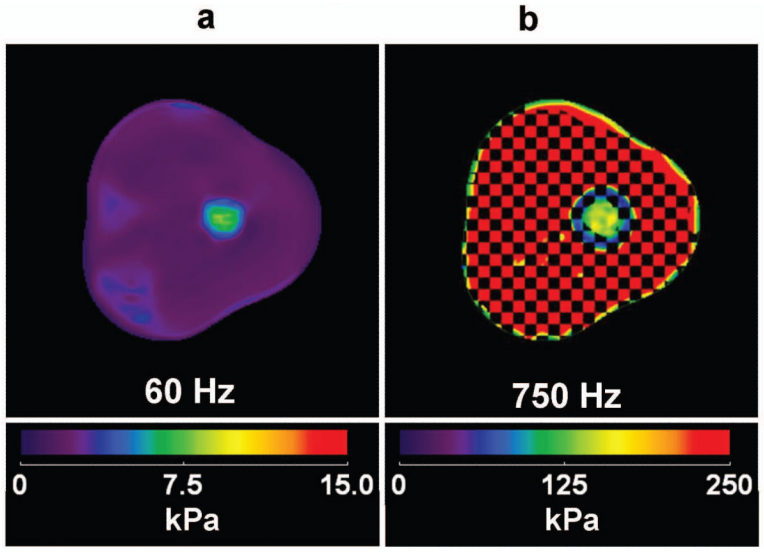

Figure 6.

(a) An elastogram of the inclusion phantom using 60-Hz shear wave data. The inclusion is detected to be stiffer than the surrounding gel, but its stiffness is significantly underestimated. (b) An elastogram obtained using the 750-Hz mode-conversion MRE data, with a wave amplitude mask indicating the regions where the stiffness values could not be trusted. The soft gel is erroneously reported as very stiff throughout much of the phantom, reasonable stiffness values are obtained close to the inclusion boundary. The stiffness reported for the stiff inclusion is much closer to the predicted value due to the shorter wavelengths of the waves at this frequency.

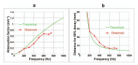

Figure 7.
(a) A graphical comparison of the theoretical (without marker) and the observed (with marker) attenuation factors for the B-gel in the inclusion phantom at various frequencies. (b) A comparison of the distance required for 99% decay of the wave amplitude for the theoretical model and the experimental observations. The measured data agree well with the theoretical model.

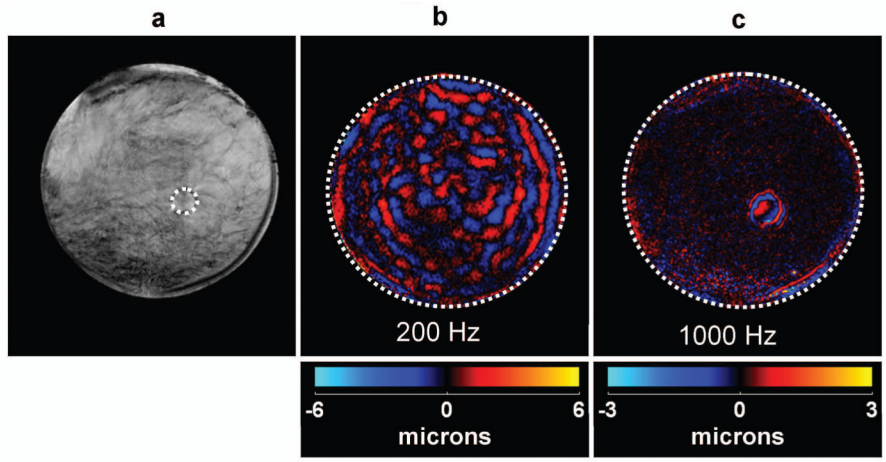

Figure 8.

(a) A conventional MR magnitude image of a breast specimen where a stiffer, FUS-ablated region is shown by the dotted line. (b) A single wave image showing mode-converted shear waves produced by 200-Hz longitudinal vibrations. The stiff region can not be seen by inspecting the wave data. (c) A wave image of mode-converted 1000-Hz shear waves showing the stiff region as clearly distinctive from the background tissue.

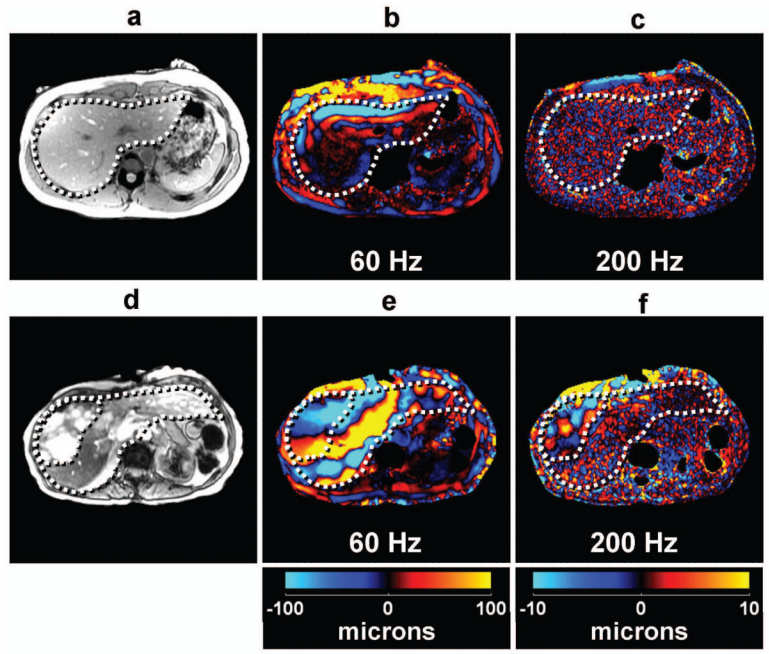

Figure 9.

Results from an in vivo hepatic study of a normal volunteer and a patient with metastatic liver tumors. Conventional MR magnitude images of the volunteer (a) and the patient (d) show the presence of numerous tumors in the patient. Wave data in the volunteer at 60 Hz (b) and 200 Hz (c) show that the shear waves at 200 Hz are completely attenuated in normal healthy soft liver tissue. The wave data in the patient at 60 Hz (e) and 200 Hz (f) show that the waves in the stiff tumors are still clearly observable while the shear waves in the rest of the liver have been significantly attenuated.